Automatic Detection of the Craniometric Points for Craniofacial Identification

LUIZ CLÁUDIO PARZIANELLO[1]
MAMEDE AUGUSTO MACHADO DA SILVEIRA[2]
SÉRGIO SHIGUEMI FURUIE[1]
FORTUNATO ANTÔNIO BADAN PALHARES[2]

[1]Heart Institute of São Paulo - HCFM-USP - Division of Informatics
Av. Dr. Enéas de Carvalho Aguiar, 44, 05403.000 São Paulo, SP, Brazil
{ parzianello, furuie }@incor.usp.br

[2]Department of Legal Medicine, FCM-UNICAMP
13081.970 Campinas, SP, Brazil

Abstract. An automatic method for the detection of craniometric points in video based skull images is presented. This method assumes that skull images are in frontal view and erect posture of the head. An acquisition protocol is described, that facilitates the segmentation process. Although the proposed method uses simple algorithms of the image processing theory, it produces good results for undamaged skulls and is potentially very useful in the craniofacial identification process.

Keywords: Medical Imaging, Craniofacial Identification.

1 Introduction

In the middle of 1990, a clandestine common grave was found at the Dom Bosco cemetery in Perus, City of São Paulo, which contained 1,048 skeletons of individuals who had died from 1971 to 1974. Since the remains of missing political activists were thought to be among them, some families and Human Rights committees requested the mayor's office to identify those who were buried in the common grave. Several entities and universities were invited to join in the work, and a team of physicians, students, photographers, cinematographers, engineers and system analysts was assembled.

The skeletons were first labelled, packed, photographed and filmed, and questionnaires were distributed to family members to describe physical and anthropometric features of each missing person [Palhares et al. (1995a)]. To date, five political activists have been identified, all by means of the *image superimposition technique*.

Due to the large number of skeletons found and the long time required to identify each missing person, it became desirable to build an automatic anthropometric identification system to accelerate this process. In this paper we present a method designed to automatically locate craniometric points in digitised skull images, thus aiding skilled specialists in the craniofacial identification process.

The Craniofacial Identification

It was Brash who first suggested that photographs of missing person and skulls could be superimposed as an identification technique [Brash-Glaister (1937) apud Sekharam (1993)]. A human skull can be identified as belonging to a missing person if some common characteristics are unique, or more precisely, if the probability of confusing it with another skull is very low [Schimmler et al. (1993)].

Some important anatomic anthropometric features of a human skull are relevant in the identification process [Palhares et al. (1995b)]. These features are called craniometric points and represent the primary information considered in this procedure (Figure 1). The reliability of skull identification based on a set of craniometric points depends heavily on the individuality of the skulls expressed in terms of these craniometric points.

The classical superimposition technique is based on a time-consuming manual and empirical process. First, the digitised photographic portrait of the person is visualised on a video screen, and the craniometric points are estimated on the person's face by a specialist. The same craniometric points are then identified and marked on the skull image, acquired by a digital camera. The probability of the correspondence between the set of points measured on the skull, and their equivalent points measured on the photographic portrait, is then evaluated using a procedure described in [Palhares et al. (1995b)]. If the correlation among the two sets of points is high, the recognition of the skull is positive.

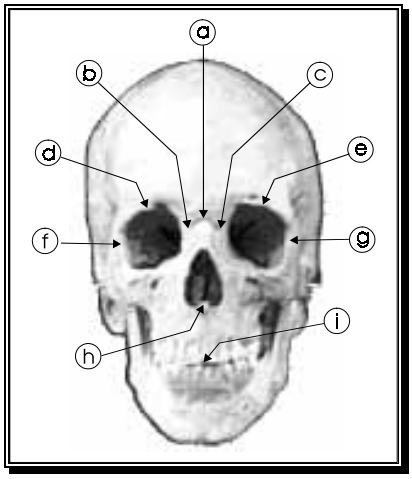

Figure 1. (a) *Nasion*, the midpoint of the suture between the frontal and the two nasal bones; (b) right and (c) left *dacryons*, the points of junction of the frontal, maxillary, and lachrymal bones on the medial wall of the orbit; (d) right and (e) left *orbitalis superius*, upper point of eye socket; (f) right and (g) left *orbitalis horizontalis*, the most lateral point of the lateral wall of the orbit; (h) *nasospinale*, the point where a line drawn between the lower margins of the right and left nasal apertures is intersected by the midsagittal plane; (i) *incisor superius*, the tip of the crown of the most anterior maxillary central incisor.

Automatic methods to determine both sets of points are of great use in departments that analyse large amounts of data for identification purposes. Our aim is to design an automatic procedure to determine craniometric points in non-damaged skull images. The method includes some constraints during image acquisition, is easy to implement and fast to process.

2 Methods

In most cases Forensic Science is based on empirical data discovered in autopsy studies. Since there are no general geometric rules to define the location of the craniometric points, morphological features estimated through statistical analysis are considered. The automatic detection procedure then consists of a number of simple image processing steps.

Pre-processing

Both noise reduction and removal of small artefacts from an image are common tasks in image processing techniques prior to object segmentation [Gonzales-Woods (1992)]. Noise reduction by blurring with a linear filter is suitable for analogue video camera acquisitions.

For our purpose, a simple 5x5 spatial averaging mask is used to reduce the influence of spurious data, simplifying the segmentation technique. The result of the convolution mask can be expressed as:

$$f'(x,y) = \frac{1}{25} \sum_{j=-2}^{2} \sum_{i=-2}^{2} f(x+i, y+j), \qquad (1)$$

where $f(x,y)$ is the original image and $f'(x,y)$ is the filtered one.

Linear histogram stretching is then applied over the grey scale in order to improve image contrast. Figure 9a illustrates the result of the two operations performed in sequence.

Regions of Interest Segmentation

Since the skulls are always positioned in frontal view and erect posture of the head (see Acquisition Protocol, in section 3), the craniometric points are found through segmentation of four particular regions: the whole skull region, the two orbital cavities, and the nasal cavity.

With normal illumination, these regions are defined by two grey level thresholding operations: one at 20% of the maximum (removing the background, supposed to be entirely contained in this range), and one at half-maximum (targeting orbital and nasal regions). The results of both segmentations are illustrated in Figures 2a and 2b.

Figure 2. (a) Skull segmentation with grey level thresholding at the 20% grey level and (b) at the middle level.

Skull contour determination is based on the image thresholded at 20 % of the maximum. A starting point of the contour is found as the first non null point on the vertical median line of the thresholded image, starting from the top. The contour is then found by inner border determination with an inner boundary tracing algorithm [Sonka-Hlavac (1993)], and is used to compute the centroid and vertical axis of the skull in a reliable way (Figure 3a).

The centroid is given by the first moment of the contour:

$$\bar{x} = \frac{\sum\sum x.Co(x,y)}{\sum\sum Co(x,y)} \quad (2)$$

and

$$\bar{y} = \frac{\sum\sum y.Co(x,y)}{\sum\sum Co(x,y)}, \quad (3)$$

where $(\bar{x},\bar{y})$ are the coordinates of the centroid and *Co(x,y)* is the skull contour. The vertical axis is defined as the vertical line through the $\bar{x}$ coordinate.

A logical combination of the external contour with the image of the cavities, found from mid-scale thresholding, results in a useful image for labelling purposes. The cavities image being represented by *Ca(x,y)*, the combination of both images may be written as:

$$C(x,y) = \left[Co(x,y) \cup Ca(x,y)\right]^c, \quad (4)$$

where $\cup$ is the logical union and ^{c} is the logical complement (Figure 3b).

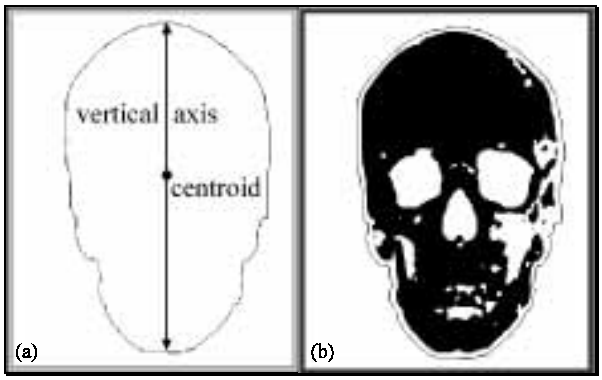

Figure 3. (a) Representation of the skull centroid and vertical axis over the contour determined through the inner boundary tracing algorithm (the image is shown in negative to facilitate visualisation). *(b)* The logical combination of the external contour image and the cavities image.

Craniometric Points Identification

The location of each orbital cavity was found by morphological analysis. A set of skull images was presented to an expert, who marked the centre of each orbit (medium point). The mean distance between each cavity centre and the skull centroid was computed, and normalised by dividing by the length of the vertical axis. This normalisation ensures a non-dimensional measurement for different sizes of skulls. These radial co-ordinates, as well as the mean angular co-ordinates of both orbit centres with respect to the vertical axis are shown in Table 1 and Figure 4.

TABLE 1: Morphological Analysis of the Skull

Element to centroid	**Distance/Vertical Length**
left orbit centre	0.1633 ± 0,0176
right orbit centre	0.1522 ± 0,0126
Element to vertical axis	**Tilt**
left orbit centre	+72.90° ± 11.50°
right orbit centre	-72.25° ± 10.80°

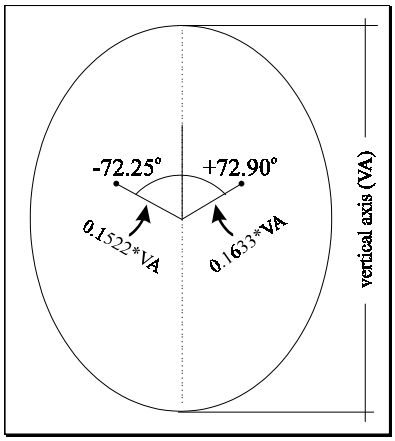

Figure 4. Graphic representation of the relationships between the vertical axis and the location of each orbital cavity centre.

For each skull, these centre points serve as the centres of two angular searches in the binary image $C(x,y)$, where 64 binary radial profiles are built in order to find 64 edges along each orbital contour. Based on the hypothesis that boundaries of orbital cavities are defined as closed curves, we assume that they can be described by a Fourier expansion with a limited number of harmonics.

Let us express the simple closed contour *l* in polar co-ordinates (r,θ) with respect to an origin *P* within the convex area bounded by *l*; the monotonous radial mapping function is given by $r = L(\theta)$ (Figure 5).

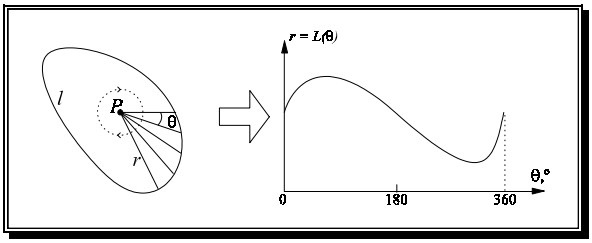

Figure 5. A contour radial mapping referenced to an internal point of the closed contour.

Three harmonics were found sufficient to recover the profile of normal orbital cavities, while smoothing any abrupt variation resulting from the thresholding operation (Figure 9b). Thus, the new contour becomes:

$$L(\theta) = \frac{a_0}{2} + \sum_{i=1}^{3}\left[a_i.\cos(i.\theta) + b_i.\sin(i.\theta)\right]. \quad (5)$$

As is shown in Figure 9b, the estimated orbital centres are not in the middle of each orbit and the

smoothed contour does not match the orbital boundaries. However, the angular frequency components in equation (5) are independent of the position of the centre, and the estimated orbital contours are no more than a preliminary step in the identification of the craniometric points.

Therefore, calculating the new middle points for each orbital contour, we get better approximations to the orbital centres, and can now derive the orbital craniometric points:

- *orbitalis superius*: considering a vertical line segment from the orbital centre to the top, with a length twice the distance between the middle orbital point and the top of the orbital contour, *orbitalis superius* is located at the point of maximum vertical derivative along this vertical line segment.

•located at the point of maximum vertical derivative along the vertical line segment from the orbital centre to the top, the length of which is twice the distance between the middle orbital point and the orbital contour.

- *orbitalis horizontalis*: located at the point of maximum horizontal derivative along the line segment between the middle orbital point and the left (or right) side of the skull contour.

- *dacryons*: located at the point of maximum horizontal derivative along the line segment between the middle orbital point and the skull vertical axis.

A point in the nasal cavity is determined by the intersection of the skull vertical axis and the horizontal line through the lowest point of both orbital contours. The same procedures as for the orbital contours are applied to the nasal contour, including Fourier filtering. Figure 9c illustrates the determination of the orbital craniometric points and the nasal contour after Fourier filtering. The nasal craniometric points are determined as follows:

- *nasion*: located at the point of maximum vertical derivative along the skull vertical axis, within the segment limited by the highest point of the two orbital contours and the lowest dacryon.

- *nasospinale*: located at the lower intersection of the skull vertical axis with the nasal contour.

The above procedures are illustrated in Figure 9.

The algorithm to determine the location of the incisor superius point is under development; simple geometrical considerations are not sufficient to guarantee the correct localisation of this point. Another concern is related to damaged skulls and toothless individuals, in which case the incisor superius point must be located without any derivative information around its neighbourhood. Figure 6 shows an example of a toothless individual where the incisor superius point was marked manually.

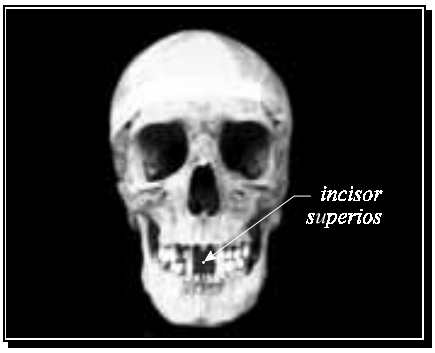

Figure 6: An example where there is no derivative information for the incisor superius location.

3 Apparatus

A set of 10 skulls of adult humans was used to evaluate the proposed algorithm. The samples were collected from Perus skeletons and the nine craniometric points were marked by a specialist (F.A.B.P.).

A mechanical device is used to adjust the position of each skull for digital image acquisition. Three stepping motors allow rotation around three axes; the step size of each motor (Dynasyn, model 68090) is 1.8°, reduced at a ratio of 800:1 by a system of gears attached to it. Each motor is computer controlled, using a special interface and software (Eletromaq mod. ELT9425), which result in a high precision skull positioning device.

The skulls are supported mechanically by one screw in each auditory cavity (Figure 7). The mechanical support and the background wall are covered with a dark non-reflective material (black velvet, e.g.) to facilitate the segmentation procedure.

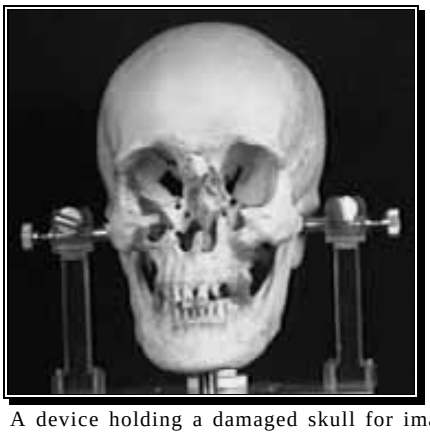

Figure 7: A device holding a damaged skull for image capture.

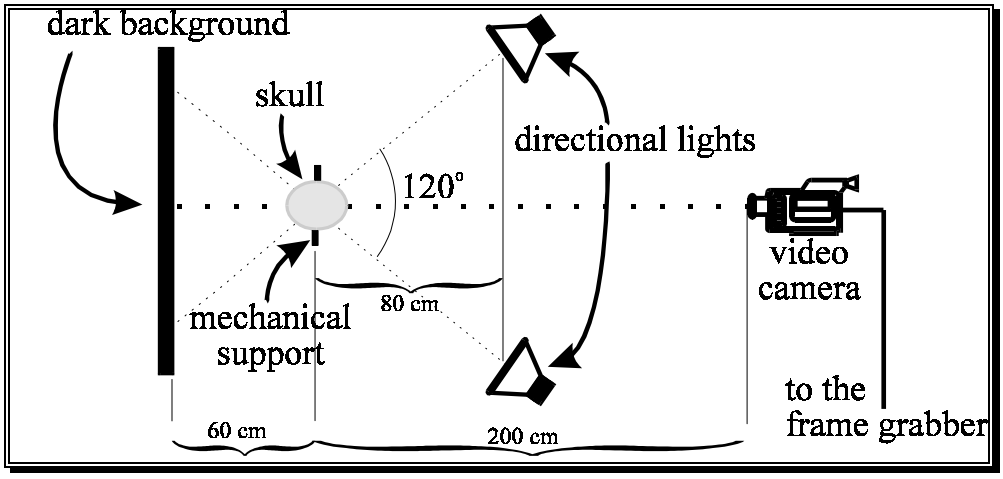

Figure 8: Physical distribution of the equipment in the laboratory.

A Hitachi KP-C501 video camera, connected to a personal computer (486DX-40MHz) using a Targa AT-Vista frame grabber, is used to acquire the images with a spatial resolution of 640 x 480 pixels and a pixel depth of 8 bits for all cases.

The algorithm was implemented in the C language using AVS (Application Visualization System) as a development platform, and was run and evaluated on a Sun Sparc10 station.

Acquisition Protocol

Considering the simplicity of the proposed algorithm, several conditions are imposed to the acquisition protocol. The reflections on the background and the mechanical support must be minimised, and a correspondingly dark and non-reflective material must be used to cover these areas. This allows all background to be removed by the 20 % thresholding step.

The skull has to be illuminated by a bi-directional light to avoid lightening the orbital and nasal cavities. Two 150 W white directional lamps, placed at an angle of 120° in front of the skull, produce a uniform illumination of the skull.

Finally, the skull must best fill out the entire size of the acquired frame, thus minimising unwanted background contributions. Figure 8 is a schematic illustration of the distribution of the acquisition apparatus in the laboratory.

4 Results and Discussions

Statistical observations have shown that the orbital cavities may be reliably located by the use of non-dimensional polar co-ordinates, centred at the centroid of the skull contour. A method was found to yield the orbital and nasal craniometric points based on simple geometrical considerations.

Acquiring the images under controlled conditions allowed us to use simple image processing techniques, such as thresholding and radial mapping of the contour. Global shape information of the cavities' contours was incorporated into the segmentation process through angular filtering in the Fourier domain.

Visual inspection by a specialist showed that the localisation of the orbital and nasal craniometric points yielded satisfactory results in all ten cases that were investigated.

However, a full validation of this method requires a quantitative evaluation: taking account of inter- and intra-operator variability figures, as well as studying a larger sample population, classified according to age, sex and ethnic origin of the indivuals. Populations of different ethnic origins present systematic anthropometric differences, and these characteristics would merit a more detailed investigation. Moreover, further investigations are necessary to obtain accurate localisation of the *incisor superius* point, regardless of the physical presence of the incisor and the inferior jaw bone. A more complex system allowing the localisation of craniometric points on damaged skulls, such as the one shown in Figure 7, is another possible future development of the present method.

6 Conclusion

Fully automated processes in forensic analysis accelerate the work of the experts and permit faster identification of missing persons or suspects. Automatic estimation of the craniometric points on the face, or automatic registration of skull images with photographic portraits, are but a few examples of useful potential applications

of image processing techniques to the Forensic Sciences, and are certainly worth some investigation.

In conclusion, our method for the automatic detection of craniometric points on digital skull images produced good results; it was designed as an aid in the craniofacial identification procedure, as part of an anthroprometric system still under development.

ACKNOWLEDGEMENT

We are most grateful to Dr. Matthias Egger for his inestimable collaboration revising the paper.

References

F.A.B. Palhares, S.L. Olivier, M.A.M. Silveira, A.C.C. Monteiro, J.E.B Zappa, L.B.P Gerson, "Utilizing the Superimposition Technique in Identity Determination the Perus's Skeletons Example", *Forensic Odontology & Anthropology*, in Advances in Forensic Sciences V.7, ed. K.W. Alt & P. Pieper, Verlag Dr. Köster, 1995a.

F.A.B. Palhares, M.A.M. Silveira, S.L. Olivier, C.L. Tozzi, A.M.G. Tommaselli, J.K. Hasegawa, "A Model for Evaluating the Correspondence in the Craniofacial Identification Process", *Forensic Odontology & Anthropology*, in Advances in Forensic Sciences V.7, ed. K.W. Alt & P. Pieper, Verlag Dr. Köster, 1995b.

J.B. Schimmler, R.P. Helmer, J. Rieger, "Craniometric Individuality of Human Skulls", in *Forensic Analysis of the Skull*, ed. M.Y. Iscan & R.P. Helmer, Wiley-Liss, 1993.

P.C. Sekharam. "Positioning the Skull for Superimposition", in *Forensic Analysis of the Skull*, ed. M.Y. Iscan & R.P. Helmer, Wiley-Liss, 1993.

R.C. Gonzales, R.E. Woods, *Digital Image Processing*, Addison-Wesley, 1992.

M. Ekman, M. Lomsky, S.O. Strömblad, S. Carlsson, "Closed-Line Integral Optimization Edge Detection Algorithm and Its Application in Equilibrium Radionuclide Angiocardiography", *The Journal of Nuclear Medicine*, 6 (1995), 1914 - 1018.

Figure 9. (a) Skull image after application of the local averaging mask and linear histogram stretching. (b) Smoothing orbital profiles by angular Fourier filtering. The figure shows the new profiles and the centre estimations; (c) Orbital craniometric points determination and nasal contour estimation by angular Fourier filtering. (d) Nasal craniometric points determination.